DTU Library

A neutron scattering and electron microscopy study of the structure, wetting, and freezing behavior of water near hydrophilic CuO-nanostructured surfaces

Torres, J.; Buck, Z. N.; Kaiser, H.; He, X.; White, T.; Tyagi, M.; Winholtz, R. A.; Hansen, F. Y.; Herwig, K. W.; Taub, H.

J. Torres ⒾⒹ, Z. N. Buck ⒾⒹ, H. Kaiser, X. He, T. White, M. Tyagi, R. A. Winholtz, F. Y. Hansen, K. W. Herwig ⒾⒹ, and H. Taub ⒾⒹ

View Online   Export Citation   CrossMark

A neutron scattering and electron microscopy study of the structure, wetting, and freezing behavior of water near hydrophilic CuO-nanostructured surfaces

J. Torres,[1] [ID] Z. N. Buck,[1] [ID] H. Kaiser,[1] X. He,[2] T. White,[2] M. Tyagi,[3,4] R. A. Winholtz,[5] F. Y. Hansen,[6] K. W. Herwig,[7] [ID] and H. Taub[1,a] [ID]

AFFILIATIONS

[1]Department of Physics and Astronomy and Research Reactor, University of Missouri, Columbia, Missouri 65211, USA
[2]Electron Microscopy Core Facility, University of Missouri, Columbia, Missouri 65211, USA
[3]Center for Neutron Research, National Institute of Standards and Technology, Gaithersburg, Maryland 20899, USA
[4]Department of Materials Science and Engineering, University of Maryland, College Park, Maryland 20742, USA
[5]Department of Mechanical and Aerospace Engineering, University of Missouri, Columbia, Missouri 65211, USA
[6]Department of Chemistry, Technical University of Denmark, IK 207 DTU, DK-2800 Lyngby, Denmark
[7]Neutron Technologies Division, Oak Ridge National Laboratory, Oak Ridge, Tennessee 37831, USA

[a]Author to whom correspondence should be addressed: taubh@missouri.edu

ABSTRACT

Oscillating heat pipes (OHPs) provide a promising heat transfer device for a variety of applications, including the cooling of electronic devices. Recently, it has been shown that a hydrophilic, nanostructured cupric oxide (CuO) coating can significantly enhance the thermal performance of copper OHPs that use water as the working fluid. Motivated by these results, we report neutron scattering and electron microscopy (EM) measurements to investigate the interaction of water with copper-oxide surfaces on the nanoscale. Our measurements confirm earlier observations of a thin cuprous oxide (Cu_2O) layer growing on a bare copper substrate followed by "grass-like" CuO nanostructures. New evidence of the nanostructure hydrophilicity is provided by EM measurements of wetting and by our high-energy-resolution elastic neutron scattering measurements, showing a continuous freezing and melting of the water in our samples over a temperature range of ~80 K. In addition, our neutron diffraction measurements are consistent with water closest to the CuO nanostructures freezing into an amorphous solid at low levels of hydration and hexagonal ice at higher hydration. In short, our findings support a strong interaction of water with the CuO nanostructures, which could significantly affect the operation of an OHP.

I. INTRODUCTION

Invented in the 1990s, oscillating heat pipes (OHPs) offer a promising heat transfer device for a variety of applications, including the cooling of electronic devices.[1] An OHP contains a channel meandering between a heat source (evaporator) and heat sink (condenser) that can either be made of small-diameter tubing or fabricated from a flat plate with a milled channel. The OHP is sealed, evacuated, and partially backfilled with a working fluid, which results in evaporation and condensation at opposite ends of the OHP due to heat addition and heat rejection, respectively. If the channel diameter of the OHP is sufficiently small to support capillary action, then liquid "slugs" and vapor "bubbles" will form within the channel. Pressure differences within the system drive the oscillating motion of these slugs and bubbles, enabling both sensible and latent heat transfer from the evaporator to the condenser.[1]

Recently, it has been shown that, for a flat-plate copper OHP operating with water as the working fluid, a hydrophilic coating of CuO nanostructures on either the evaporator or condenser sections can enhance its thermal performance as measured by a reduction in the temperature difference between the heat source and sink.[2,3] Despite the demonstration that such a CuO coating improves heat-transfer performance, the microscopic mechanisms responsible for this enhancement remain unknown.

The interaction of water with strongly hydrophilic, porous surfaces has received increasing attention in the last two decades with numerous review articles (see, e.g., Refs. 4–8). For the most part, these reviews have emphasized the macroscopic characterization of hydrophilic surfaces (e.g., by water contact angle measurements),[5–8] the role of both surface chemistry and surface roughness in enhancing hydrophilicity,[5–8] the fabrication of hydrophilic materials,[4–8] and applications of these materials.[4–8] However, compared to water near atomically smooth, planar surfaces,[9–12] there has been less attention paid to determining the molecular-scale structure of water that is near hydrophilic surfaces in *porous* materials. Most of these studies have been limited to water interacting with the hydrophilic surfaces within mesoporous[13,14] and nanoporous[15] silicas and silica-like materials.[16] Both the structure of water and its freezing/melting behavior when confined within the pores of these materials have been investigated.

In this paper, we use neutron scattering techniques to probe the structure and dynamics of water in proximity to porous and strongly hydrophilic CuO surfaces, which have a qualitatively different topography than the cylindrical pores within the silicas. We find that the water near the nanostructured CuO surfaces exhibits a continuous melting/freezing transition spanning a temperature range that extends 80 K below the bulk transition at 273 K. Also, on slow cooling of our low-hydration samples, we obtain evidence of amorphous solid water forming near a temperature of 240 K. These features differ qualitatively from that of water near ideal, planar metal-oxide surfaces[12] for which the water structure can be described in terms of three structurally distinct layers.

As discussed in Sec. II, we use both electron microscopy and neutron scattering to probe the water structure near the CuO nanostructures. These techniques allow us to investigate the wetting behavior and melting/freezing transitions as well as the structure of the solid water at the molecular level.

II. EXPERIMENTAL

A. Electron microscopy and water contact angle measurements

To mimic the copper surfaces in a flat-plate OHP, we used thin (12.7 μm) copper foil as a substrate (All Foils, USA[17]). CuO nanostructures were prepared on the foil using a wet chemical method.[18] The foils were cleaned in acetone, etched in 2.0 M hydrochloric acid to remove the native oxide layer, and then immersed in a pH-14 solution consisting of NaClO$_2$,

NaOH, Na$_3$PO$_4$·12H$_2$O, and deionized water in the ratio 3.75:5:10:100 by weight. After a 10-min exposure to solution at ~368 K, the foils were rinsed several times in deionized water and air-dried.

To characterize the copper-oxide morphology and crystallinity, we used a combination of scanning electron microscopy (SEM) and transmission electron microscopy (TEM) at the University of Missouri Electron Microscopy Core Facility. We prepared a TEM sample using a lift-out method in a focused-ion-beam SEM instrument (FEI Scios Analytical). An oxidized-copper-foil cross section ~100 nm thick was transferred to a 300 keV TEM (FEI Tecnai F30 Twin) equipped with a Gatan image filter. Electron energy-loss spectroscopy (EELS), scanning-TEM imaging, and selected-area electron diffraction (SAED) were used to characterize the chemical composition and structure of the sample. The EELS energy resolution was 1 eV based on the full-width at half-maximum of the zero-loss peak.

We determined the millimeter-scale surface wettability of untreated and CuO-coated copper foils by water contact-angle measurements (Ramé-Hart Model 200), using 1 μl droplets of purified water under ambient conditions. Results were averaged over several (3-10) droplets on different samples.

In addition, we investigated micron-scale surface wettability using an environmental-SEM instrument (FEI Quanta 600F) at a saturated water vapor pressure of 500 Pa. Foil samples of size 1×1 cm^2 were mounted at an angle of ~15° to the primary-beam direction on custom-made oxygen-free high-conductivity (OFHC) copper stubs. We adjusted the electron beam accelerating voltage (5-20 kV), sample-detector gap distance (10-15 mm), image dwell time (0.3-30 μs), water vapor pressure (~500 Pa), and sample temperature (268–293 K) for the best signal-to-noise ratio. Similar to the technique used by others,[19] by lowering the sample temperature below 271 K at a pressure of 500 Pa, we could condense supercooled water on untreated-copper surfaces and the CuO nanostructures. Images were formed by electrons backscattered into a gaseous electron detector both before and after the observation of liquid water. Recording ended when the water layer thickness exceeded the escape length of backscattered electrons. Reproducibility was confirmed by repeating condensation and evaporation cycles on several samples.

B. Elastic neutron intensity measurements

Our neutron scattering samples consisted of 100 copper foil disks, each 5 cm in diameter. A large number and diameter of the foils were necessary to increase the scattered neutron intensity from the water layer on each side of the foils. The foil thickness (12.7 μm) was chosen to decrease the incoherent scattering from the copper substrates. The foils were stacked in a cylindrical aluminum can in a helium atmosphere and sealed with an indium O-ring. Prior to sealing, samples were heated to ~328 K in air for 48 h to remove excess water. In the sample of untreated copper, aluminum foil rings (5 cm outer diameter, ~4.8 cm inner diameter, and ~22.9 μm thick) were interlaid between copper foils to increase the stack

height in order to fill the incident neutron beam cross section (30×30 mm^2). Sample hydration was established by a water droplet of known volume (H$_2$O for incoherent elastic scattering and D$_2$O for neutron diffraction); it was placed outside of the neutron scattering volume using a micropipette before sealing (see Fig. 1).

The freezing/melting behavior of the water in our samples was observed by measuring the temperature-dependence of the intensity of neutrons scattered elastically from the sample. In our samples, the incoherent scattering from the H atoms in the water molecules dominates the elastic signal. We used the High-Flux Backscattering Spectrometer (HFBS)[20] at the NIST (National Institute of Standards and Technology) Center for Neutron Research, which has an energy resolution of ~1μeV. An increase in the elastically scattered neutron intensity on this instrument is proportional to an increase in the number of H atoms which are either immobile or moving on a time scale longer than ~4 ns. Therefore, at low temperatures, the elastic intensity provides a measure of the amount of immobilized water in our samples.[21] To increase the scattering signal, the elastic intensity was summed over all 16 detectors, which cover a wave vector transfer (Q) range of 0.25 Å$^{-1} < Q < 1.75$ Å^{-1}, and then normalized to the incident beam monitor located in front of the sample position. Cooling and heating scans were taken at a rate of 0.08 K/min between 200 K and 280 K for three different samples: CuO-nanostructured copper foils with 60 μl of H$_2$O; a similar sample with 10 μl of H$_2$O; and, to serve as a control, untreated-copper foils with 60 μl of H$_2$O. These water volumes were selected based on previous proof-of-concept measurements on the HFBS as well as from our earlier work on single-supported bilayer lipid membranes.[21] In practice, a volume of 10 μl yielded the smallest quasielastic intensity from water that could be analyzed.
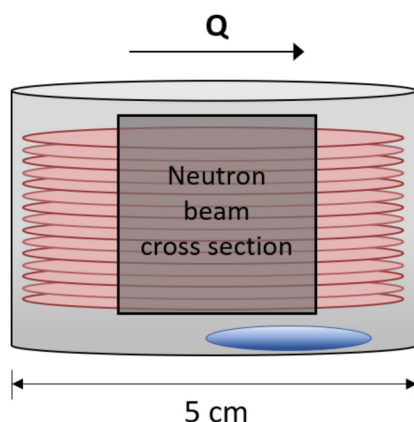

FIG. 1. Sketch of the sample cell used for neutron scattering experiments. A water droplet (H$_2$O or D$_2$O) of known volume placed at the bottom of the cell, outside of the neutron scattering volume, controls the hydration level. The scattering vector **Q** lies in the plane of the copper foils. The incident neutron beam cross section has dimensions 30×30 mm^2. Not drawn to scale.

C. Neutron diffraction

To determine the structure and composition of the copper-oxide coatings and their associated water, we conducted neutron diffraction measurements on a two-axis diffractometer equipped with five position-sensitive detectors at the University of Missouri Research Reactor (MURR).[22] The incident neutron wavelength was 1.485 Å. The samples used in these diffraction measurements were identical to those used for the incoherent elastic scattering experiments except that they were hydrated with D$_2$O instead of H$_2$O (120 μl or 240 μl) to enhance the coherent scattering from the water. A third sample, which had no added D$_2$O, was also measured to determine background scattering. Diffraction patterns were taken in temperature steps of 5 K from ~295 K to 200 K in search of Bragg peaks from crystalline ice.

III. RESULTS AND DISCUSSION

A. Structure of the copper-oxide coating

The physical and chemical properties of CuO nanostructures depend on the synthesis conditions under which they are grown (e.g., ion concentration, temperature, time).[23] Using the recipe by Nam and Ju,[18] the CuO nanostructures formed a "grass-like" morphology, uniformly coating the copper substrate. A comparison of the untreated-copper and CuO surfaces is given in the SEM images in Figs. 2(a) and 2(b), respectively, with a magnified view of the CuO grass-like morphology in Fig. 2(c). The dimensions of each triangular CuO blade are typically ~2 μm tall, ~0.5 μm wide at the base, and ~20 nm thick.

To observe the layered structure of the CuO coating on copper foil, we have used high-spatial-resolution TEM. A cross-sectional view of a foil is shown in the high-angle dark-field (HAADF) image in Fig. 3(a). HAADF images are formed primarily by backscattered electrons collected at relatively large angles with respect to the incident beam. In principle, the gray-scale intensity of each pixel of an HAADF image is proportional to Z^2, where Z is the average atomic number.[24] Thus, an HAADF image can be analyzed to determine differences in chemical composition between layers in a sample. The approximate average Z^2 values for Cu, Cu$_2$O, and CuO are 841, 484, and 342, respectively. Accordingly, the gray-scale intensity of bulk copper would appear brightest, CuO the darkest, and Cu$_2$O in between, consistent with Fig. 3(a). The black areas in Fig. 3(a) are holes in the sample through which the incident beam passes unimpeded.

Selected-area electron diffraction (SAED) patterns were taken within the circled region at the lower interface in Fig. 3(a). The pattern in Fig. 3(b) shows Bragg spots indicative of single-crystal domains, which could be indexed to bulk copper and cuprous oxide (Cu$_2$O).[25] Moreover, the diffraction patterns reveal a complete epitaxial relationship between the Cu and Cu$_2$O layers: Cu[112]‖Cu$_2$O[112]; Cu(111)‖Cu$_2$O(111); and Cu(220)‖Cu$_2$O(220) as has been observed previously.[26]

EELS scans, collected simultaneously with STEM images, were used to identify chemical composition within each layer
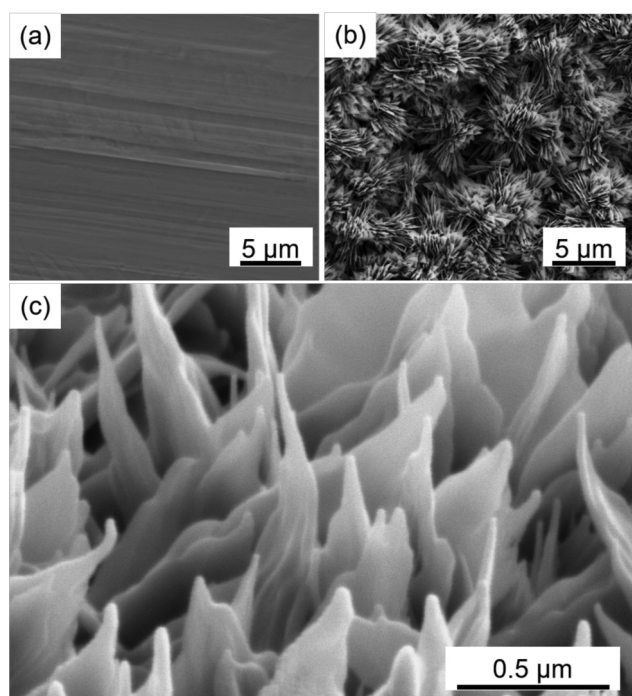
FIG. 2. Typical SEM images of (a) untreated-copper foil and [(b) and (c)] CuO nanostructures. Striations in (a) are produced during the manufacturing process (rolling). The magnified image (c) of the CuO coating shows the grass-like oxide morphology.

labeled in Fig. 3(a). Representative scans are shown in Fig. 3(c). In these scans, the incident electron beam excites the sample's electrons into vacant states above the ionization edges of copper's core-shell electrons.[27] The shapes of the L-transitions (2p to 3d shell) near 931 eV and 951 eV and their intensity ratio (L_3-to-L_2) can be used to fingerprint the oxidation state of metallic copper and its compounds.[25] The shapes of the EELS edges agree well with those reported elsewhere[28] and, together with HAADF images [Fig. 3(a)] and SAED patterns [Fig. 3(b)], confirm the identity of the layers as labeled in Fig. 3(a).

Our neutron diffraction measurements provided additional evidence of the three layers (Cu, Cu_2O, and CuO). Samples of untreated and CuO-coated copper foils were prepared as illustrated in Fig. 1. Room-temperature diffraction scans are plotted in Fig. 4. The untreated-copper contains Bragg peaks indexed to fcc copper as well as a few weak aluminum Bragg peaks contributed by the vertical spacers between copper foils. In addition to bulk copper, two copper-oxide phases were found in the treated sample: cubic Cu_2O and monoclinic CuO. The weakness of the Cu_2O and CuO peak intensities is consistent with the thinness of the oxide layers identified by electron microscopy in Fig. 3(a).
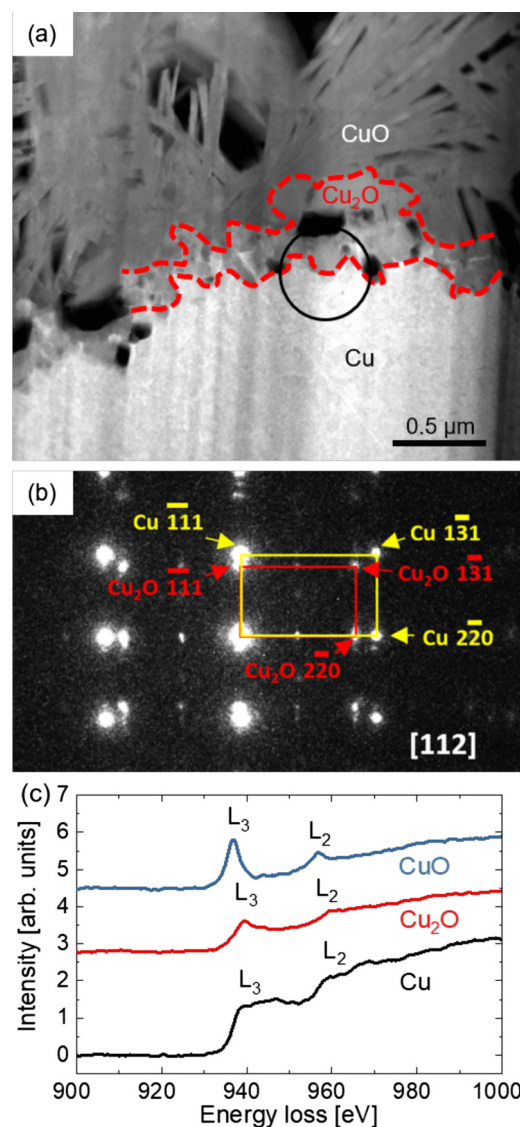
FIG. 3. (a) HAADF image of the layers (Cu, Cu_2O, and CuO) in a cross-sectional view of the sample. Identification of the layers is based on image contrast, enabling the Cu_2O region to be outlined by the dashed red lines. The average estimated thickness of the Cu_2O layer, normal to the copper substrate, is 216 ± 98 nm in agreement with Ref. 5. (b) SAED pattern taken in the region enclosed by the black circle in (a) along the [112] zone axis of both Cu and Cu_2O. (c) Background-subtracted EELS scans taken within the three layers identified in (a) with the copper L_2 and L_3 edges labeled. Spectra are offset vertically for clarity. The vertical streaking in (a) is due to variations in sample thickness caused by inhomogeneous ion-milling during the lift-out procedure.

B. Wetting behavior

Micro- and nano-structuring of surfaces can enhance wetting[5–8,18,23] as was found for the CuO coating used in flat-plate copper OHPs.[2,3] Our water contact-angle measurements show that untreated copper is relatively hydrophobic

FIG. 4. Background-subtracted room-temperature neutron diffraction patterns for CuO-coated copper foil (thick line) and untreated-copper (thin line). Bragg peaks are labeled with their corresponding Miller indices and colored according 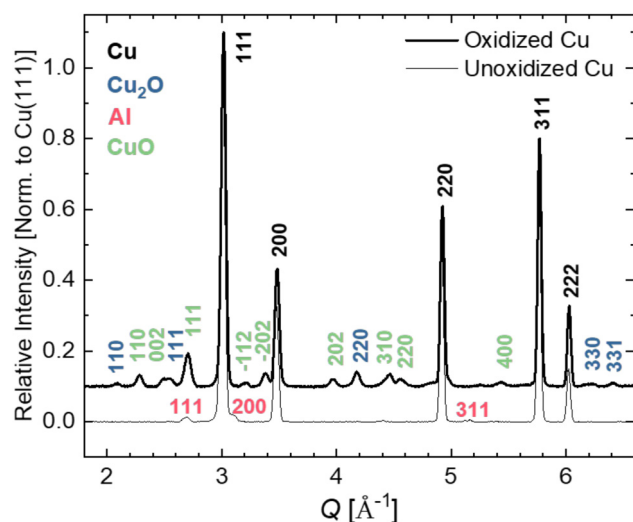to phase: Cu (black), Cu_2O (blue), Al (pink), and CuO (green). Intensity of the two samples is normalized to the most intense Bragg peak, Cu (111). The pattern for the CuO-coated copper foil is offset vertically for clarity.

with equilibrium contact angles of $\sim 70°$ [Fig. 5(a)]. In contrast, water droplets deposited on the CuO coating, similar to that in Figs. 2(b) and 2(c), immediately spread to contact angles of $\sim 0°$ [Fig. 5(b)], which is characteristic of superhydrophilic surfaces.[5]
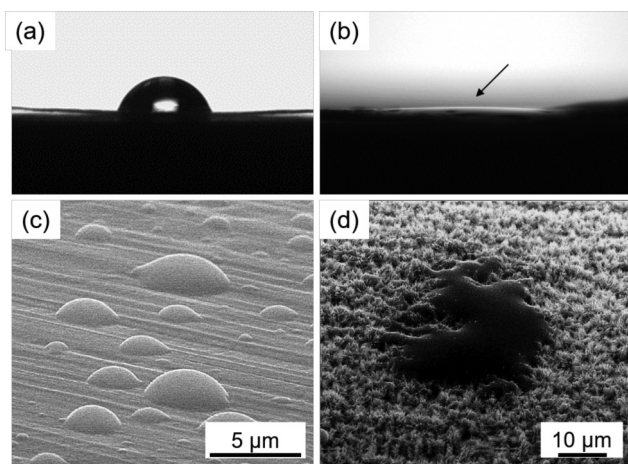

FIG. 5. Equilibrium water contact-angle measurements, using 1μl droplets, for (a) untreated-copper and (b) CuO surfaces with average values of 70° and $\sim 0°$, respectively. The arrow in (b) points to the water droplet that spreads on the CuO surface. Observation by environmental SEM of water condensation on (c) untreated copper and (d) CuO surfaces.

In addition to water contact-angle measurements, we have used environmental-SEM (ESEM) water-condensation experiments to elucidate the differences in the wetting behavior of water on untreated-copper and CuO surfaces. ESEM images were obtained by collecting backscattered electrons as the beam performs a raster scan across the surface. As in TEM-HAADF imaging [see Fig. 3(a)], the intensity of an SEM-backscattered-electron image depends on the Z of the target atoms. High-Z materials have a greater probability of elastically scattering electrons than low-Z materials and thus appear brighter, although topographic variations in these samples can modulate the image intensity. The advantages of ESEM are the ability to create a humid environment similar to that within our neutron scattering sample cell (Fig. 1) and to determine droplet shapes of micron size.

Representative ESEM images for untreated-copper [Fig. 5(c)] and CuO-nanostructured surfaces [Fig. 5(d)] were taken during the condensation process. On the untreated-copper surface, we observed hemispherically-shaped droplets that retained their shape throughout nucleation and subsequent growth. In contrast, water that condensed on the hydrophilic CuO coating nucleated near the base of the nanostructures and formed a thin film which increased in thickness as condensation proceeded. When the water reached the top of the CuO blades, it formed a hemispherical shape, like the droplets on untreated-copper surfaces, but with the droplet edges pinned to the CuO blades. We note that in addition to the grass-like blades of the CuO surfaces promoting capillary condensation, the presence of OH groups on the nanostructures may enhance their affinity for water.

C. Freezing and melting behavior

In addition to observations of the wetting behavior of the CuO nanostructures, the strength of their interaction with water can also be assessed by investigating their effect on the water freezing transition. Differential scanning calorimetry (DSC) is frequently used to investigate the freezing and melting behavior of water confined in porous media (see, e.g., Ref. 14). We have tried to apply the DSC technique to our system, but the specific surface area of our CuO-coated samples ($\sim 0.6 \, m^2/g$) is so small that a DSC sample contains an amount of water that is two to three orders of magnitude less than the quantity typically used (a few mg) in measurements with commercial DSC instruments. For this reason, we have been unable to perform reliable DSC scans to investigate the continuous freezing/melting behavior of our samples.

Due to the large incoherent cross section of hydrogen and the large size of our neutron scattering samples (see Fig. 1), our elastic neutron scans provide greater sensitivity than DSC for investigating the continuous freezing/melting behavior observed in our samples. Also, we note that the elastic neutron scans are sensitive only to the motion of water molecules on a time scale slower than $\sim 4 \, ns$ whereas the DSC scans integrate molecular motion over a wider range of time scales.

Figure 6 contains our elastic neutron scans on three samples: (a) CuO-coated foils with $60\,\mu l$ of added H_2O, (b) CuO-coated foils with $10\,\mu l$ of H_2O, and (c) untreated copper foils with $60\,\mu l$ of H_2O. For all three samples, each data point is the intensity measured in a counting time of five minutes during which the sample temperature changed by 0.4 K as determined by the temperature ramp rate of 0.08 K/min on cooling and on heating. The intensity of the high-hydration CuO-coated sample [Fig. 6(a)] gradually increased when slow-cooled from 280 K to 200 K. On heating at the same rate from 200 K to 280 K, hysteresis was observed, and the intensity
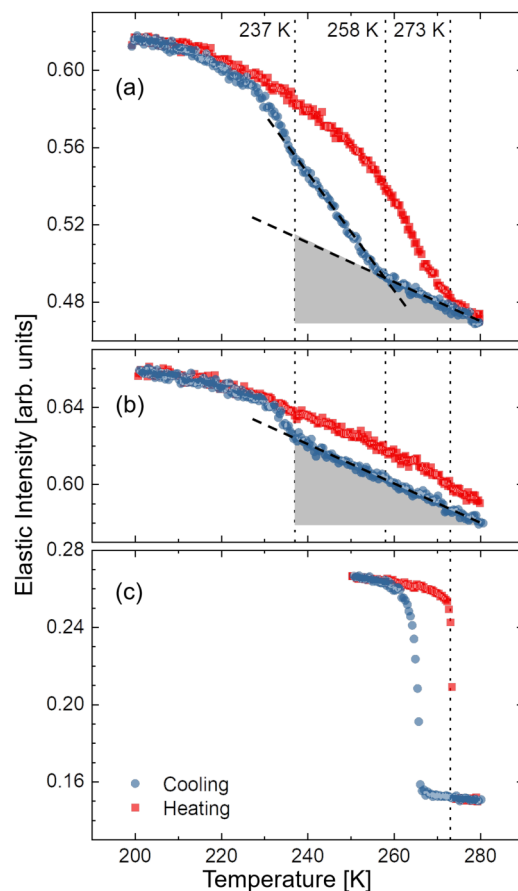

FIG. 6. Elastic neutron scattered intensity vs. sample temperature, summed over all detectors ($0.25\,\text{Å}^{-1} < Q < 1.75\,\text{Å}^{-1}$), upon cooling (blue circles) and heating (red squares) for three samples: (a) CuO-coated foils with $60\,\mu l$ of H_2O added, (b) CuO-coated foils with $10\,\mu l$ of H_2O, and (c) untreated copper foils with $60\,\mu l$ of H_2O. Vertical dotted lines are drawn at 237 K and 258 K, corresponding to inflection points in the cooling curves of (a) and (b) (see text), and at 273 K, the melting point of bulk ice. In (a) and (b), the dashed lines are guides to the eye. The two shaded triangles are identical and indicate the temperature range and slope of the linear term in (b). One sees that the initial slope of the intensity is the same in (a) and (b) for the high- and low-hydration CuO-coated samples. The vertical scale is the same for each panel to facilitate comparison of intensities.

gradually decreased. We have interpreted this behavior as representing continuous freezing and melting of water that is interacting with the CuO nanostructures. A similar trend was found in the low-hydration CuO-coated sample [Fig. 6(b)], although the hysteresis is reduced and the intensity difference between 200 K and 280 K is about half that of the high-hydration CuO-coated sample in Fig. 6(a). We note that this intensity decrease is less than the volume ratio 1:6 of the initial water droplets added to the two samples. Assuming that all of the initial water droplet is adsorbed onto the CuO-coated foils (see below), there are several possible reasons for this discrepancy: irreproducibility in the amount of residual water on the foils after annealing the samples and variation in their surface area and hydrophilicity.

In marked contrast, the elastic scan for the untreated-copper sample [Fig. 6(c)], conducted at the same cooling rate as the CuO-coated samples, shows an abrupt intensity increase near 266 K below which the intensity levels off. On slow heating, the intensity decreases sharply at the melting point of bulk ice, 273 K.

On closer inspection of the elastic scans of the low-hydration CuO-coated sample [Fig. 6(b)], we find that, on cooling, the elastic intensity obeys a linear dependence from 280 K down to ∼237 K. Similarly, the intensity of the high-hydration sample [Fig. 6(a)] has a linear dependence initially with the same slope as the low-hydration CuO-coated sample; however, this behavior ends at ∼258 K. As will be discussed further below, this initial linear term occurring in the freezing behavior of both samples, having different levels of hydration, suggests that they share a common water population confined to a similar local environment.[21]

On cooling below 258 K, the elastic intensity of the high-hydration CuO-coated sample again increases linearly but with a larger slope than initially. This linear dependence extends down to ∼237 K, the temperature at which the linear dependence of the intensity in the low-hydration sample ends. We suggest that both linear terms contribute to the intensity of the high-hydration CuO-coated sample in the temperature range 237 K < T < 258 K. The presence of a steeper linear term in the elastic intensity scan of this sample provides evidence of a second water population occupying a distinct nanoscale environment. Presumably, this second population is located further away from the copper substrate but still confined within the CuO nanostructures above which water is expected to exhibit bulk-freezing characteristics.

To quantify the hydration level in our samples, we estimate the number of immobilized water molecules from the increase in elastic intensity on cooling from 280 K to 200 K. This number is determined by calibration against a standard sample of an alkane film, containing a known number of H atoms, that freezes on a silicon substrate.[21] A correction is applied for the larger incoherent cross section of our predominantly copper substrates relative to silicon. Assuming that the water wetting the CuO surface forms a uniform film as suggested by the ESEM image in Fig. 5(d), we find an upper bound to the water film thickness of the high- and low-

hydration samples to be ~200 nm and ~100 nm, respectively. Although the uncertainty in these estimates is large, we believe it is reasonable to conclude that the film thickness is less than the typical height of a CuO blade, ~2 μm. These film thickness estimates imply water volumes of ~80 μl and ~40 μl adsorbed on the CuO coatings of the high- and low-hydration samples, respectively. For both samples, these volumes exceed those in the initial droplet, suggesting the presence of residual water after the samples were annealed.

The continuous freezing behavior observed for water in proximity to the CuO-nanostructured surfaces differs from that which we have found for water near other interfaces. For example, the water associated with an anionic bilayer lipid membrane also exhibited a continuous freezing behavior, but its elastic scan on cooling began with a step-like feature, somewhat broader than we have found for our untreated-copper sample in Fig. 6(c) and whose magnitude increased with the water content of the sample (see Fig. 3 in Ref. 29). This behavior suggested identifying it with the freezing of bulk-like water as was subsequently verified by measurement of its diffusivity.[21] Such a step-like feature is missing in the case of water associated with the CuO-coated samples [Figs. 6(a) and 6(b)], suggesting the absence of bulk-like water.

There are reports of continuous freezing of interfacial water in other porous materials. Liu et al.[15] observed elastic scans from water confined to mesoporous silica that show a gradual increase in elastic intensity from 300 K down to 150 K. Also, Mamontov et al.[30] found qualitatively similar freezing behavior in elastic scans from samples of water adsorbed in ultramicroporous carbon. As in the case of our samples, they observe the intensity to increase linearly with temperature on cooling below room temperature at low relative humidity.[30] However, unlike our two samples [see Figs. 6(a) and 6(b)], the slope of this initial linear term increases with water content, suggesting a greater amount of a single water type confined in the micropores. At the highest relative humidity, the temperature dependence of the elastic intensity is initially concave upward, perhaps indicating the condensation of bulk-like water within the larger pores.

D. Structure of the solid water

The elastic scans in Fig. 6 are useful for determining whether the water in a sample is liquid or solid and the nature of its freezing/melting transitions. However, the incoherent elastic intensity gives no direct information about the structure of the solid water. To determine whether the water in proximity to CuO nanostructures freezes into crystalline ice (e.g., hexagonal or cubic), we performed neutron diffraction measurements at MURR on similarly fabricated samples (see Fig. 1) except that D_2O was substituted for H_2O to enhance the coherent scattering from the water.

Due to the weak intensity expected for Bragg peaks from crystalline ice, we began our measurements with samples of untreated-copper and CuO-nanostructured foils containing 120 μl of D_2O. As shown in Fig. 7(a), the pattern for the untreated-copper sample contains the first three peaks
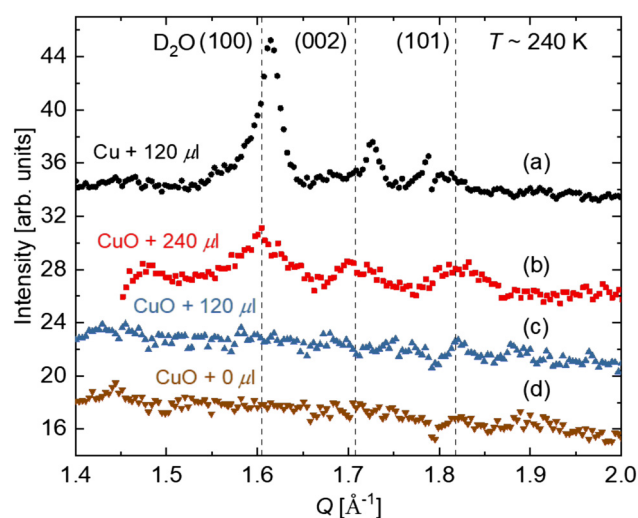

FIG. 7. Neutron diffraction scans at ~240 K vs. wave vector transfer Q for four samples: (a) untreated-copper foils with 120 μl of D_2O (black circles); (b) CuO-coated sample with 240 μl of D_2O (red squares); (c) CuO-coated sample with 120 μl of D_2O (blue triangles); and (d) CuO-coated sample without added D_2O (tan down triangles). Vertical lines are drawn at Q values corresponding to the first three Bragg reflections observed for bulk hexagonal D_2O ice at 240 K:[31] (100), (002), and (101). Patterns are offset vertically for clarity.

expected for hexagonal ice,[31] which appear on cooling near 272 K or about 5 K below the freezing point of bulk D_2O. However, no peaks are visible for the CuO-coated sample containing the same amount of water [Fig. 7(c)]. The pattern is virtually identical to that of the sample containing no D_2O [Fig. 7(d)]. The maximum uncertainty in the temperature measurement is ~2 K, based on a temperature gradient between the temperature sensors at the top and bottom of the sample cell.

We then dismounted the CuO-coated sample, heated it in air at ~328 K for 24 h, and resealed it with 240 μl of D_2O. A subsequent diffraction scan [Fig. 7(b)] shows the same three Bragg peaks of hexagonal ice for the untreated sample [Fig. 7(a)]. We interpret these results as indicating the growth of hexagonal ice at higher D_2O coverage. No Bragg peaks that could be identified with cubic ice were present in repeated scans on the nanostructured samples. In this respect, our results differ from measurements on water confined to mesoporous silica where evidence of cubic as well as hexagonal and disordered ice have been found.[13,14] The larger width of the peaks in Fig. 7(b) compared to those in Fig. 7(a) indicates a smaller crystallite size and/or a larger mosaic structure than for the untreated-copper sample—a feature that may be caused by the water film thickness being less than the height of the CuO nanostructures. From the observed broadening of the D_2O (100) peak below 260 K, the average domain size of the ice particles is estimated to be ~30 nm based on a Scherrer analysis.

The absence of Bragg peaks at lower D_2O coverages could be explained by water initially solidifying in an amorphous or glassy structure. We suggest that the most favorable candidate for amorphous solid water would be the first water population identified in the elastic scans of both the high- and low-hydration samples, whose intensity has the smaller slope on cooling [see Figs. 6(a) and 6(b)]. Because it is the first to immobilize, indicating the strongest interaction with the CuO nanostructures, this population should be the most likely to form a distorted network of hydrogen bonds that is incompatible with crystalline ice. This interpretation is consistent with our ESEM images [see Fig. 5(d)], which show water to condense first near the base of the nanostructures where the density of the CuO blades is the highest. However, it is possible that the second water population identified in the elastic scan of the high-hydration sample and believed to be further from the base of the blades might also freeze into an amorphous structure. Its higher level of hydration ($60 \mu l$ of D_2O added) is still less than that at which the Bragg peaks of hexagonal ice appeared ($240 \mu l$). It is interesting to note that previous investigations of water freezing in mesoporous silicas have found evidence of disordered ice in a layer adjacent to the pore walls in which the local hydrogen bonding of the water molecules is believed to differ from that of bulk ice.[13,14] Similarly, Mamontov *et al.*[30] concluded that water adsorbed in partially filled pores of their ultramicroporous carbon samples did not crystallize on cooling, which they attributed to a disruption of its hydrogen bonding network.

It is well known that metal-oxide surfaces exposed to humid air adsorb water and form hydroxyl (–OH) groups. The hydroxide reaction at the copper surface during oxidation is likely a source of –OH as well. The H atoms in these surface components will scatter neutrons incoherently, producing an isotropic background in a diffraction measurement. Consistent with this effect, we found that at all temperatures, the background intensity in the diffraction patterns of both CuO-coated samples was greater than that of the untreated-copper hydrated sample, especially at low Q ($<0.5 \text{ Å}^{-1}$). This higher background of the CuO-coated samples did not depend on their hydration level ($120 \mu l$ or $240 \mu l$ of added D_2O). A higher background due to bound water and hydroxyl groups might also explain the larger elastic intensity of the CuO-coated samples at 280 K [Figs. 6(a) and 6(b)] compared to the untreated-copper sample [Fig. 6(c)].

In Fig. 8(a), we show the temperature dependence of diffraction patterns from the CuO-coated sample hydrated with $240 \mu l$ of D_2O taken subsequently to the pattern in Fig. 7(b). As before, the Bragg peak positions are consistent with bulk hexagonal D_2O ice.[31] In addition, we find that the intensity of the three Bragg peaks does not increase abruptly but rather grows continuously. This behavior can be seen more clearly in Fig. 8(b), where we have plotted the integrated intensity of the D_2O (100) peak obtained in a Gaussian fit as a function of temperature. As indicated by the dashed line, the peak intensity increases roughly linearly on cooling from 260 K to 230 K. Below 230 K, the Bragg peak intensity levels off consistent with the crystallization of all of the bulk-like water. The full-
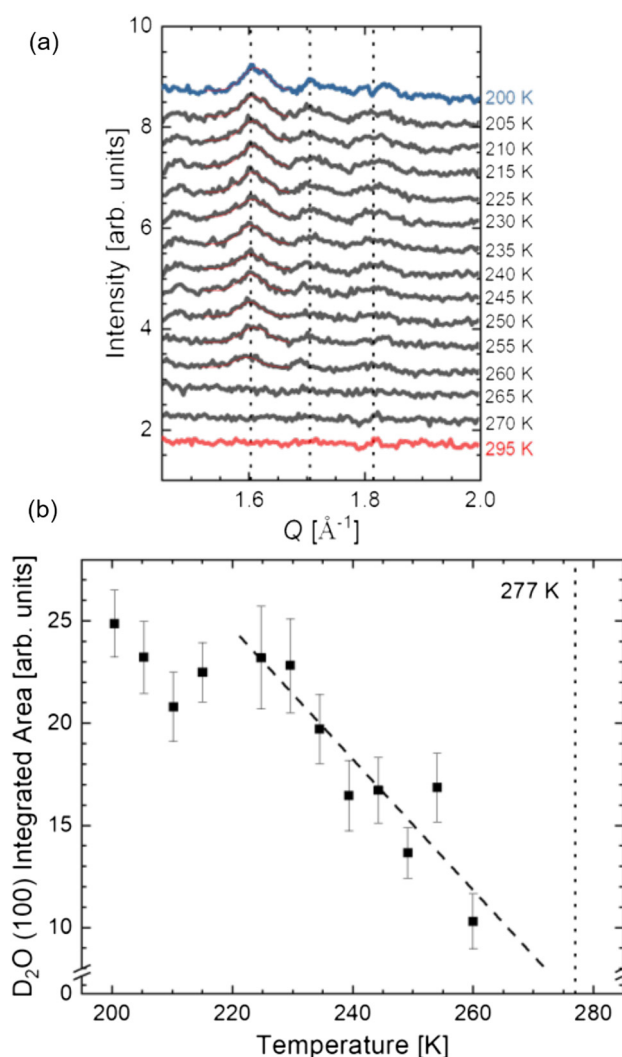

FIG. 8. (a) Temperature dependence of the neutron diffraction patterns from the CuO-coated sample hydrated with $240 \mu l$ of D_2O on cooling from 295 K to 200 K. Dotted vertical lines are drawn at Q values corresponding to the first three Bragg reflections observed for bulk hexagonal D_2O ice at 265 K.[31] The diffraction patterns are offset vertically for clarity. (b) Temperature dependence of the D_2O (100) Bragg peak intensity determined from a Gaussian fit to the peaks in (a). The dashed line is a least-squares fit to the points between 230 K and 260 K. Error bars represent one standard deviation in the uncertainty of the intensity. A vertical dotted line is drawn at the melting point of bulk D_2O, 277 K.

width at half-maximum of the (100) peak has a flat temperature dependence over the entire temperature range of Fig. 8(b) (not shown) from which we can conclude that ice growth on the CuO surface proceeds through nucleation of additional ice particles rather than by coalescence.

We also note that the linear dependence of the Bragg peak intensity occurs in the same temperature range as that observed for the incoherent elastic intensity of the

high-hydration CuO sample [see Fig. 6(a)]; but, as these samples are hydrated to different levels and are measured on different types of instruments, it is virtually impossible to relate the slopes of these linear terms. This comparison would be interesting, recalling that the intensity of the incoherently and elastically scattered neutrons is proportional to the amount of *immobilized* water in the sample (on a time scale of ~4 ns), whereas the Bragg intensity in Fig. 8(b) is proportional to the amount of *crystalline* water.

Presumably, the crystallization of bulk hexagonal D_2O ice is the result of freezing bulk-like water. Yet, as discussed above, the continuous elastic scans of both CuO samples [Figs. 6(a) and 6(b)] provided no direct evidence of bulk-like water, and no Bragg peaks were observed in the diffraction pattern of the CuO sample hydrated to $120\,\mu l$ of D_2O as seen in the untreated-copper sample. Therefore, we hypothesize that increasing the hydration level from $120\,\mu l$ to $240\,\mu l$ introduces a bulk-like water component near room temperature located further from the base of the CuO blades where their density is lower.

IV. SUMMARY AND CONCLUSIONS

We have confirmed earlier findings that an untreated metallic copper surface, when exposed to an alkaline environment, oxidizes to form first a thin layer of Cu_2O followed by grass-like CuO nanostructures. For water confined within these layers, we find evidence of a strong interaction with the CuO nanostructures as indicated by its wetting behavior on the microscale (Fig. 5) and by its continuous freezing and melting transitions, extending over a wide temperature range, $200\,K < T < 280\,K$ (Fig. 6).

An analysis of the water freezing behavior exhibited by the elastic scans of the CuO-coated samples [Figs. 6(a) and 6(b)] provides evidence of two different water populations: (1) a component that is present in samples hydrated with $10\,\mu l$ and $60\,\mu l$ of H_2O and presumed to be located nearest to the copper substrate [see Fig. 3(a)] and (2) a second component, which is present only in the sample hydrated with $60\,\mu l$ of H_2O and hence likely to be located above the first. At neither level of hydration do the elastic scans of the CuO-coated samples have the characteristic initial upward step on cooling, which we attribute to bulk-like water as in the case of the untreated-copper sample [Fig. 6(c)] and in bilayer lipid membrane samples.[21] Quasielastic and inelastic neutron scattering measurements are now in progress, which should assist in determining the dynamics of the different water populations in both their solid and liquid states.[32]

We have observed Bragg peaks at a low temperature characteristic of crystalline D_2O in the neutron diffraction pattern of the untreated-copper sample. However, they are absent in a CuO-coated sample hydrated to the same level ($120\,\mu l$) but appear at higher hydration ($240\,\mu l$). These results suggest that water in closest proximity to the CuO nanostructures may solidify initially in an amorphous solid or glassy phase.

At this point, we can only speculate as to how the presence of the CuO coating could enhance the thermal performance of an OHP. It may be that superwetting of water to the CuO nanostructures not only facilitates heat transfer to and from the working fluid in an OHP but also changes the boundary condition for water flow at the pipe wall that could alter the amplitude and frequency of the water slug oscillations. The evidence that we have found for an amorphous solid or glassy phase of water at low temperatures suggests that water in contact with the CuO nanostructures could form a dynamic hydrogen-bond network in its fluid phase differing from that of bulk water at the same temperature. In fact, our preliminary quasielastic neutron scattering measurements[32] indicate the presence of slower molecular diffusive motion than in bulk water. It would be interesting to investigate whether these microscopic dynamical effects correlate with changes in the amplitude and frequency of the water slug oscillations in an OHP caused by a CuO coating as has been observed by Hao et al.[33] Thus, combining quasielastic neutron scattering on CuO-coated foils with neutron imaging on an operating OHP[3] may lead to a better understanding of how a CuO coating enhances OHP thermal performance.

REFERENCES

[1] Y. Zhang and A. Faghri, Heat Transf. Eng. **29**, 20 (2008).
[2] Y. Ji, C. Xu, H. Ma, and P. Xinxiang, J. Heat Transf. **135**, 074504 (2013).
[3] F. Z. Zhang, R. A. Winholtz, W. J. Black, M. R. Wilson, H. Taub, and H. B. Ma, J. Heat Transfer **138**, 062901 (2016).
[4] E.-P. Ng and S. Mintova, Microporous Mesoporous Mater. **114**, 1–26 (2008).
[5] J. Drelich, E. Chibowski, D. D. Meng, and K. Terpilowski, Soft Matter **7**, 9804 (2011).
[6] B. Su, Y. Tian, and L. Jiang, J. Am. Chem. Soc. **138**, 1727 (2016).
[7] T. A. Otitoju, A. L. Ahmad, and B. S. Ooi, J. Indus. Eng. Chem. **47**, 19 (2017).
[8] L. Zhang, N. Zhao, and J. Xu, J. Adhesion Sci. Technol. **28**, 769 (2014).
[9] A. Verdaguer, G. M. Sacha, H. Bluhm, and M. Salmeron, Chem. Rev. **106**, 1478 (2006).
[10] Q. Li, J. Song, F. Besenbacher, and M. Dong, Acc. Chem. Res. **48**, 119 (2015).
[11] O. Björneholm, M. H. Hansen, A. Hodgson, L.-M. Liu, D. T. Limmer, A. Michaelides, P. Pedevilla, J. Rossmeisl, H. Shen, G. Tocci, E. Tyrode, M.-M. Walz, J. Werner, and H. Bluhm, Chem. Rev. **116**, 7698 (2016).
[12] E. Mamontov, L. Vlcek, D. J. Wesolowski, P. T. Cummings, W. Wang, L. M. Anovitz, J. Rosenqvist, C. M. Brown, and V. G. Sakai, J. Phys. Chem. C **111**, 4328 (2007).

[13]J. B. W. Webber, J. C. Dore, J. H. Strange, R. Anderson, and B. Tohidi, J. Phys. Condens. Matter **19**, 415117 (2007).

[14]J. Jelassi, H. L. Castricum, M.-C. Bellissent-Funel, J. Dore, J. B. W. Webber, and R. Sridi-Dorbez, Phys. Chem. Chem. Phys. **12**, 2838 (2010).

[15]L. Liu, A. Faraone, C.-Y. Mou, C.-W. Yen, and S.-H. Chen, J. Phys. Condens. Matter **16**, S5403 (2004).

[16]F. G. Alabarse, J. Haines, O. Cambon, C. Levelut, D. Bourgogne, A. Haidoux, D. Granier, and B. Coasne, Phys. Rev. Lett. **109**, 035701 (2012).

[17]Certain commercial equipment, instruments, or materials (or suppliers) are identified in this paper to foster understanding. Such identification does not imply recommendation or endorsement by the National Institute of Standards and Technology, nor does it imply that the materials or equipment identified are necessarily the best available for this purpose.

[18]Y. Nam and Y. S. Ju, J. Adhesion Sci. Technol. **27**, 2163 (2013).

[19]X. Chen, J. Shu, and Q. Chen, Sci. Rep. **7**, 46680 (2017).

[20]A. Meyer, R. M. Dimeo, P. M. Gehring, and D. A. Neumann, Rev. Sci. Instrum. **74**, 2759 (2003).

[21]A. Miskowiec, Z. N. Buck, F. Y. Hansen, H. Kaiser, H. Taub, M. Tyagi, S. O. Diallo, E. Mamontov, and K. W. Herwig, J. Chem. Phys. **146**, 125102 (2017).

[22]R. Berliner, D. F. R. Mildner, J. Sudol, and H. Taub, *Position Sensitive Detection of Thermal Neutrons* (Academic, New York, 1983), p. 120.

[23]Q. Zhang, K. Zhang, D. Xu, G. Yang, H. Huang, F. Nie, C. Liu, and S. Yang, Prog. Mater. Sci. **60**, 208 (2014).

[24]P. A. Midgley, M. Weyland, J. M. Thomas, and B. F. G. Johnson, Chem. Commun. **10**, 907 (2001).

[25]K. Sun, J. Liu, and N. D. Browning, Appl. Catal. B **38**, 271 (2002).

[26]G. Zhou, L. Luo, L. Li, J. Ciston, E. A. Stach, and J. C. Yang, Phys. Rev. Lett. **109**, 235502 (2012).

[27]R. F. Egerton, Rep. Prog. Phys. **72**, 016502 (2009).

[28]G. Yang, S. Cheng, C. Li, J. Zhong, C. Ma, Z. Wang, and W. Xiang, J. Appl. Phys. **116**, 223707 (2014).

[29]A. Miskowiec, Z. N. Buck, M. C. Brown, H. Kaiser, F. Y. Hansen, G. M. King, H. Taub, R. Jiji, J. W. Cooley, M. Tyagi, S. O. Diallo, E. Mamontov, and K. W. Herwig, Europhys. Lett. **107**, 28008 (2014).

[30]E. Mamontov, Y. Yue, J. Bahadur, J. Guo, C. I. Contescu, N. C. Gallego, and Y. B. Melnichenko, Carbon **111**, 705 (2017).

[31]K. Röttger, A. Endriss, J. Ihringer, S. Doyle, and W. F. Kuhs, Acta Cryst. **B50**, 644 (1994).

[32]J. Torres, Z. N. Buck, H. Kaiser, M. Tyagi, F. Y. Hansen, K. W. Herwig, E. Mamontov, L. Daemon, M. K. Kidder, and H. Taub, "Study of the water dynamics near hydrophilic, nanostructured CuO surfaces using inelastic neutron scattering" (unpublished).

[33]T. Hao, X. Ma, Z. Lan, N. Li, Y. Zhao, and H. Ma, Int. J. Heat Mass Transf. **72**, 50 (2014).